Solid-State Electronics 112 (2015) 46–50

Contents lists available at ScienceDirect

Solid-State Electronics

journal homepage: www.elsevier.com/locate/sse

Electron mobility and spin lifetime enhancement in strained ultra-thin silicon films

Dmitri Osintsev *, Viktor Sverdlov, Siegfried Selberherr

Institute for Microelectronics, TU Wien, Gußhausstraße 27-29, A-1040 Wien, Austria

ARTICLE INFO

Article history:
Available online 14 March 2015

Keywords:
Thin silicon films
Spin relaxation
k · **p** model
Shear strain
Electron–phonon interaction
Mobility enhancement

ABSTRACT

Spintronics attracts much attention because of the potential to build novel spin-based devices which are superior to nowadays charge-based microelectronic devices. Silicon, the main element of microelectronics, is promising for spin-driven applications. Understanding the details of the spin propagation in silicon structures is a key for building novel spin-based nanoelectronic devices. We investigate the surface roughness- and phonon-limited electron mobility and spin relaxation in ultra-thin silicon films. We show that the spin relaxation rate due to surface roughness and phonon scattering is efficiently suppressed by an order of magnitude by applying tensile stress. We also demonstrate an almost twofold mobility increase in ultra-thin (001) SOI films under tensile [110] stress, which is due to the usually neglected strain dependence of the scattering matrix elements.

1. Introduction

Ongoing miniaturization of microelectronic devices pushes research to develop models which can accurately describe transport processes taking place in ultra-thin body SOI MOSFETs. Mobility enhancement in such structures is an important issue. Stress is routinely used to enhance the carrier mobility. However, it is expected that in ultra-thin SOI structures stress becomes less efficient for this purpose [1].

Spintronics is the rapidly developing and promising technology exploiting spin properties of electrons. A number of potential spintronic devices has been proposed [2,3]. Silicon, the main element of microelectronics, is also promising for spin-driven applications [4], because it is composed of nuclei with predominantly zero spin and is characterized by small spin-orbit coupling. Both factors favour to reduce the spin relaxation. However, the experimentally observed enhancement of spin relaxation in electrically gated lateral-channel silicon structures [5] could compromise the reliability and become an obstacle in realizing spin-driven devices. Deeper understanding of scattering and spin relaxation mechanisms in thin silicon films is therefore needed.

We investigate the surface roughness and electron–phonon limited electron mobility and spin relaxation in silicon films under shear strain. We show that due to the usually neglected dependence of the surface roughness scattering matrix elements on strain the electron mobility in such structures shows a two times increase with strain. Shear strain also results in a degeneracy lifting between the unprimed subbands resulting in a spin lifetime increase by at least an order of magnitude.

2. Model

In order to find the corresponding scattering matrix elements, the subband structure and the wave functions in silicon films must be calculated. For this purpose the effective **k** · **p** Hamiltonian describing the electron states in the conduction band of the two relevant [001] valleys in presence of shear strain ε_{xy}, spin–orbit interaction, and confinement potential $U(z)$ is written in the vicinity of the X-point along the k_z-axis in the Brillouin zone as [6,7]

$$H = \begin{bmatrix} H_1 & H_3 \\ H_3^\dagger & H_2 \end{bmatrix}, \tag{1}$$

where H_1, H_2, and H_3 are written as

$$H_1 = \begin{bmatrix} \frac{\hbar^2 k_z^2}{2m_l} + \frac{\hbar^2\left(k_x^2+k_y^2\right)}{2m_t} - \frac{\hbar^2 k_0 k_z}{m_l} + U(z) & 0 \\ 0 & \frac{\hbar^2 k_z^2}{2m_l} + \frac{\hbar^2\left(k_x^2+k_y^2\right)}{2m_t} - \frac{\hbar^2 k_0 k_z}{m_l} + U(z) \end{bmatrix}, \tag{2}$$

$$H_2 = \begin{bmatrix} \frac{\hbar^2 k_z^2}{2m_l} + \frac{\hbar^2\left(k_x^2+k_y^2\right)}{2m_t} + \frac{\hbar^2 k_0 k_z}{m_l} + U(z) & 0 \\ 0 & \frac{\hbar^2 k_z^2}{2m_l} + \frac{\hbar^2\left(k_x^2+k_y^2\right)}{2m_t} + \frac{\hbar^2 k_0 k_z}{m_l} + U(z) \end{bmatrix}, \tag{3}$$

$$H_3 = \begin{bmatrix} D\varepsilon_{xy} - \frac{\hbar^2 k_x k_y}{M} & (k_y - k_x \mathrm{i})\Delta_{so} \\ (-k_y - k_x \mathrm{i})\Delta_{so} & D\varepsilon_{xy} - \frac{\hbar^2 k_x k_y}{M} \end{bmatrix}. \tag{4}$$

* Corresponding author.
E-mail address: osintsev@iue.tuwien.ac.at (D. Osintsev).

http://dx.doi.org/10.1016/j.sse.2015.02.007
0038-1101/

Here $M^{-1} \approx m_t^{-1} - m_0^{-1}$, D =14 eV is the shear strain deformation potential, Δ_{so} =1.27 meV nm, m_t and m_l are the transversal and the longitudinal silicon effective masses, $k_0 = 0.15 \times 2\pi/a$ is the position of the valley minimum relative to the X-point in unstrained silicon. The unprimed subband energies and the four component wave functions are used to evaluate the scattering matrix elements and rates. The primed subbands can be described in a similar fashion [1].

We are considering the surface roughness (SR) and electron–phonon scattering mechanisms contributing to the spin and momentum relaxation.

The spin and momentum relaxation times are calculated by thermal averaging of the corresponding subbands in-plane momentum $\mathbf{K}_i$ dependent scattering rates $\tau_i(\mathbf{K}_i)$ [6,8,9] as

$$\frac{1}{\tau} = \frac{\sum_i \int \frac{1}{\tau_i(\mathbf{K}_i)} f(E_i)(1-f(E_i))d\mathbf{K}_i}{\sum_i \int f(E_i)d\mathbf{K}_i}, \tag{5}$$

$$\int d\mathbf{K}_i = \int_0^{2\pi} \int_{E_i^{(0)}}^{\infty} \frac{\mathbf{K}_i}{\left|\frac{\partial E_i}{\partial \mathbf{K}_i}\right|} d\varphi dE, \tag{6}$$

Here $f(E) = [1 + \exp((E-E_F)/k_BT)]^{-1}$, where k_B is the Boltzmann constant, T is the temperature, E_F is the Fermi energy, $E = E_i^{(0)} + E_i(\mathbf{K}_i)$, $E_i^{(0)} = E_i(\mathbf{K}_i = 0)$ is the energy of the bottom of the subband i, and

$$\left|\frac{\partial E_i}{\partial \mathbf{K}_i}\right| = \left|\frac{\partial E(\mathbf{K}_i)}{\partial \mathbf{K}_i}\right|_{\varphi,E}, \tag{7}$$

is the derivative of the subband dispersion along $\mathbf{K}_i$ at the angle φ defining the $\mathbf{K}_i$ direction. The surface roughness momentum (spin) relaxation rate in the subband i is calculated in the following way [7,9]

$$\frac{1}{\tau_i^{SR}(\mathbf{K}_i)} = \frac{2(4)\pi}{\hbar(2\pi)^2} \sum_j \int_0^{2\pi} \pi\Delta^2 L^2 \frac{1}{\epsilon_{ij}^2(\mathbf{K}_i - \mathbf{K}_j)} \frac{\hbar^4}{4m_l^2} \frac{|\mathbf{K}_j|}{\left|\frac{\partial E(\mathbf{K}_j)}{\partial \mathbf{K}_j}\right|} \cdot \left[\left(\frac{d\Psi_{i\mathbf{K}_i\sigma(-\sigma)}}{dz}\right)^* \left(\frac{d\Psi_{j\mathbf{K}_j\sigma}}{dz}\right)\right]^2_{z=\pm\frac{t}{2}} \times \exp\left(\frac{-(\mathbf{K}_j - \mathbf{K}_i)L^2}{4}\right) d\varphi. \tag{8}$$

$\mathbf{K}_i$, $\mathbf{K}_j$ are the in-plane wave vectors before and after scattering, φ is the angle between $\mathbf{K}_i$ and $\mathbf{K}_j$, ϵ is the dielectric permittivity, L is the autocorrelation length, Δ is the mean square value of the surface roughness fluctuations, $\Psi_{i\mathbf{K}_i}$ and $\Psi_{j\mathbf{K}_j}$ are the wave functions, and $\sigma = \pm 1$ is the spin projection to the [001] axis.

The intervalley spin relaxation rate contains the Elliott and Yafet contributions [8], which are calculated in the following way

$$\frac{1}{\tau_i^{LA}(\mathbf{K}_i)} = \frac{4\pi k_B T}{\hbar\rho\upsilon_{LA}^2} \sum_j \int_0^{2\pi} \frac{1}{2\pi} \frac{|\mathbf{K}_j|}{\left|\frac{\partial E(\mathbf{K}_j)}{\partial \mathbf{K}_j}\right|} \left[1 - \frac{\left|\frac{\partial E(\mathbf{K}_j)}{\partial \mathbf{K}_j}\right| f(E(\mathbf{K}_j))}{\left|\frac{\partial E(\mathbf{K}_j)}{\partial \mathbf{K}_i}\right| f(E(\mathbf{K}_i))}\right] \frac{1}{2} \cdot \int_0^t \left[\Psi^\dagger_{j\mathbf{K}_j-\sigma}(z) M' \Psi_{i\mathbf{K}_i\sigma}(z)\right]^* \left[\Psi^\dagger_{j\mathbf{K}_j-\sigma}(z') M' \Psi_{i\mathbf{K}_i\sigma}(z')\right] dz d\varphi. \tag{9}$$

Here the matrix M' is written as

$$M' = \begin{bmatrix} M_{ZZ} & M_{SO} \\ M_{SO}^\dagger & M_{ZZ} \end{bmatrix}, \tag{10}$$

$$M_{ZZ} = \begin{bmatrix} \Xi & 0 \\ 0 & \Xi \end{bmatrix}, \tag{11}$$

$$M_{SO} = \begin{bmatrix} 0 & D_{SO}(r_y - ir_x) \\ D_{SO}(-r_y - ir_x) & 0 \end{bmatrix}, \tag{12}$$

where $\Xi = 12$ eV is the acoustic deformation potential, $(r_y, r_x) = \mathbf{K}_i + \mathbf{K}_j$, and $D_{SO} = 15\ \text{meV}/k_0$ [8] with $k_0 = 0.15 \cdot 2\pi/a$ defined as the position of the valley minimum relative to the X-point in unstrained silicon. In contrast to mobility calculations, when the main contribution to (8) and (9) is due to intrasubband scattering, the spin relaxation is mostly determined by intersubband transitions.

Intrasubband transitions are important for the contributions determined by the shear deformation potential. The spin relaxation rate due to the transversal acoustic phonons is calculated as [10]

$$\frac{1}{\tau_i^{TA}(\mathbf{K}_i)} = \frac{4\pi k_B T}{\hbar\rho\upsilon_{TA}^2} \sum_j \int_0^{2\pi} \frac{1}{2\pi} \frac{|\mathbf{K}_j|}{\left|\frac{\partial E(\mathbf{K}_j)}{\partial \mathbf{K}_j}\right|} \left[1 - \frac{\left|\frac{\partial E(\mathbf{K}_j)}{\partial \mathbf{K}_j}\right| f(E(\mathbf{K}_j))}{\left|\frac{\partial E(\mathbf{K}_j)}{\partial \mathbf{K}_i}\right| f(E(\mathbf{K}_i))}\right] \frac{1}{2} \cdot \int_0^t \int_0^t \exp\left(-\sqrt{q_x^2 + q_y^2}|z - z'|\right) \cdot \left[\Psi^\dagger_{j\mathbf{K}_j-\sigma}(z) M \Psi_{i\mathbf{K}_i\sigma}(z)\right]^* \left[\Psi^\dagger_{j\mathbf{K}_j-\sigma}(z') M \Psi_{i\mathbf{K}_i\sigma}(z')\right] \cdot \left[\sqrt{q_x^2 + q_y^2} - \frac{8q_x^2 q_y^2 - (q_x^2+q_y^2)^2}{q_x^2+q_y^2}|z - z'|\right] dz dz' d\varphi, \tag{13}$$

where $\rho = 2329\ \frac{\text{kg}}{\text{m}^3}$ is the silicon density, $\upsilon_{TA} = 5300\ \frac{m}{s}$ is the transversal phonons' velocity, $(q_x,\ q_y) = \mathbf{K}_i - \mathbf{K}_j$, and M is the 4×4 matrix written in the basis for the spin relaxation rate.

$$M = \begin{bmatrix} 0 & 0 & D/2 & 0 \\ 0 & 0 & 0 & D/2 \\ D/2 & 0 & 0 & 0 \\ 0 & D/2 & 0 & 0 \end{bmatrix}. \tag{14}$$

Here D = 14 eV is the shear deformation potential.

The intravalley spin relaxation rate due to longitudinal acoustic phonons is calculated as [10]

$$\frac{1}{\tau_i^{LA}(\mathbf{K}_i)} = \frac{4\pi k_B T}{\hbar\rho\upsilon_{LA}^2} \sum_j \int_0^{2\pi} \frac{1}{2\pi} \frac{|\mathbf{K}_j|}{\left|\frac{\partial E(\mathbf{K}_j)}{\partial \mathbf{K}_j}\right|} \left[1 - \frac{\left|\frac{\partial E(\mathbf{K}_j)}{\partial \mathbf{K}_j}\right| f(E(\mathbf{K}_j))}{\left|\frac{\partial E(\mathbf{K}_j)}{\partial \mathbf{K}_i}\right| f(E(\mathbf{K}_i))}\right] \frac{1}{2} \cdot \int_0^t \int_0^t \exp\left(-\sqrt{q_x^2 + q_y^2}|z - z'|\right) \cdot \left[\Psi^\dagger_{j\mathbf{K}_j-\sigma}(z) M \Psi_{i\mathbf{K}_i\sigma}(z)\right]^* \left[\Psi^\dagger_{j\mathbf{K}_j-\sigma}(z') M \Psi_{i\mathbf{K}_i\sigma}(z')\right] \cdot \frac{4q_x^2 q_y^2}{\left(\sqrt{q_x^2+q_y^2}\right)^3} \left[\sqrt{q_x^2 + q_y^2}|z - z'| + 1\right] dz dz' d\varphi. \tag{15}$$

Here $\upsilon_{LA} = 8700\ \frac{m}{s}$ is the speed of the longitudinal phonons and the matrix is defined with (14).

The momentum relaxation time is evaluated in the standard way [9]. The electron mobility in inversion layers in [110] direction is calculated as [9]

$$\mu_{110} = \frac{e}{4\pi^2\hbar^2 k_B T n_s} \sum_i \int_0^{2\pi} d\phi \int_{E_i^{(0)}}^{\infty} dE \frac{|\mathbf{K}_i|}{\left|\frac{\partial E(\mathbf{K}_i)}{\partial \mathbf{K}_i}\right|} \cdot \left(\frac{\partial E(\mathbf{K}_i)}{\partial \mathbf{K}_i}\right)^2_{\varphi=\pi/4,E} \tau_{110}^{(i)} f(E)(1-f(E)), \tag{16}$$

where $n_s = \sum_i n_i$, n_i is the population of subband i, and $\tau_{110}^{(i)}$ is the momentum relaxation time in subband i for [110] direction.

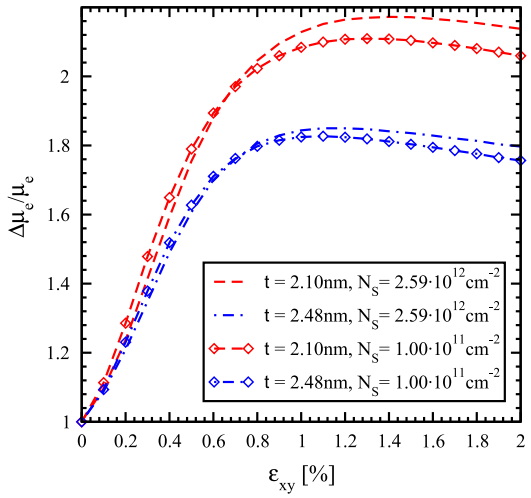

Fig. 1. Electron mobility enhancement, $\Delta\mu_e/\mu_e$, induced by shear strain as a function of strain for different thicknesses and electron concentration values for temperature 300 K.

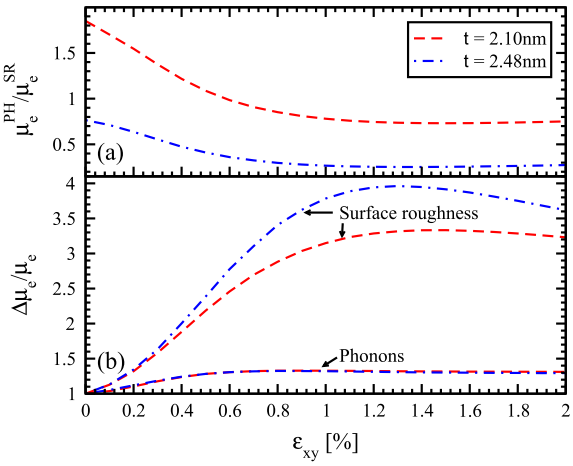

Fig. 3. Dependence of (a) the phonon electron mobility to the surface roughness mobility ratio and (b) phonon and surface roughness electron mobility enhancement on shear strain for several thicknesses for an electron concentration $2.59 \cdot 10^{12}$ cm^{-2}.

3. Discussion and results

Fig. 1 shows the electron mobility enhancement in [1 1 0] direction along tensile stress as a function of shear strain. Our results show that the mobility in thin silicon films increases by a factor of two. The increase depends on the electron concentration and the film thickness. For the thicknesses considered a strong mobility enhancement is observed up to a shear strain value around 0.5%. When the shear strain is further increased, the mobility saturates and even shows a slight decrease for the film thicknesses 2.1 nm and 2.48 nm, respectively.

The [1 1 0] mobility enhancement in surface layers due to tensile stress applied along the channel is usually explained by the effective transport mass reduction. However, the effective mass decrease in the lowest subband shown in Fig. 2 can only account for roughly one half of the mobility enhancement obtained and cannot explain the twofold mobility enhancement. Thus, a more detailed analysis is needed to understand the effect. The ratio of the phonon limited electron mobility to the surface roughness limited mobility as a function of strain is shown in Fig. 3a. The surface roughness limited mobility in the 2.1 nm thick film is of the same order as the phonon electron mobility. Thus, the total mobility is determined by the interplay between these two mechanisms. For the 2.48 nm thick film the contribution of phonons to mobility is higher than for the 2.1 nm thick film. The enhancement of the surface roughness and phonon limited mobility is shown in Fig. 3b. The phonon mobility demonstrates an increase of about 40%, which is consistent with the transport effective mass decrease. This behavior is supported by an almost negligible dependence of the electron–phonon scattering matrix elements on strain (Fig. 4).

The surface roughness (SR) limited mobility for 2.1 nm and 2.48 nm thick films rises by about 200% and 300%, respectively, at around 1.2% shear strain and shows a slight decrease at strain values higher than 1.2%. This behavior is caused by the corresponding enhancement of the inverse SR scattering matrix elements (Fig. 4). The mobility enhancement shown in Fig. 3b and the ratio shown in Fig. 3a are consistent with the total mobility enhancement observed in Fig. 1. Indeed, for the $t = 2.1$ nm film the unaccounted mobility enhancement is mostly due to the SR mobility increase. Although the SR mobility growths even stronger for $t = 2.48$ nm, the main contribution to limit the mobility is the phonon scattering. For this reason the whole mobility is slightly less enhanced as compared to that in the $t = 2.1$ nm film.

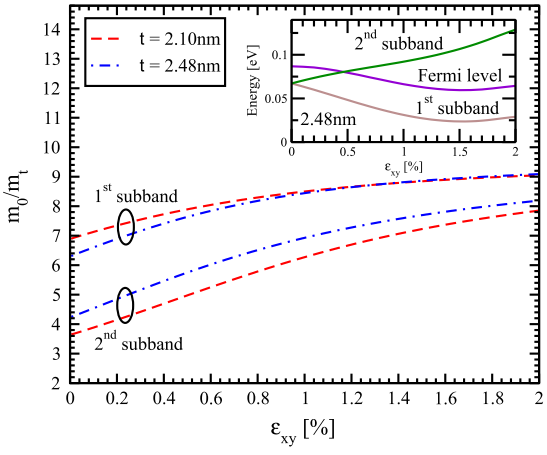

Fig. 2. Normalized reciprocal effective mass for the two lowest subbands as a function of shear strain for different film thicknesses. The inset shows the subbands energies and the Fermi level as a function of shear strain.

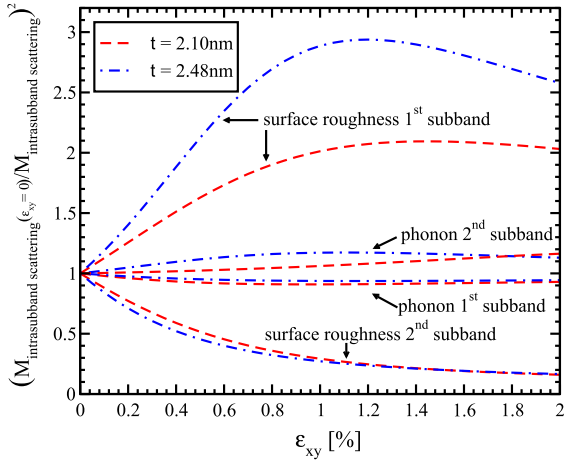

Fig. 4. Dependence of the reciprocal normalized square of surface roughness and phonon intrasubband matrix elements for different film thicknesses.

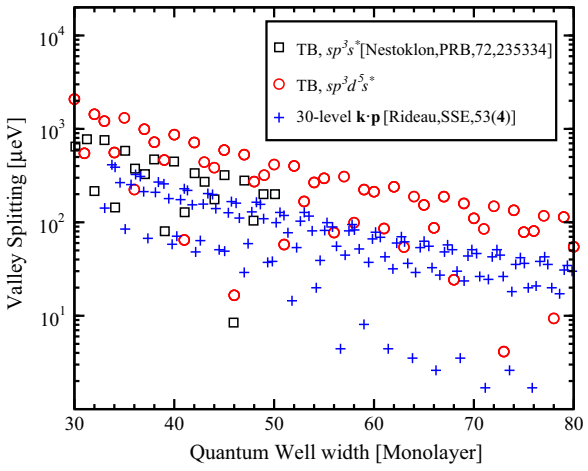

Fig. 5. Valley splitting in a Si quantum well at zero strain as a function of the quantum well width including results from literature [6,8].

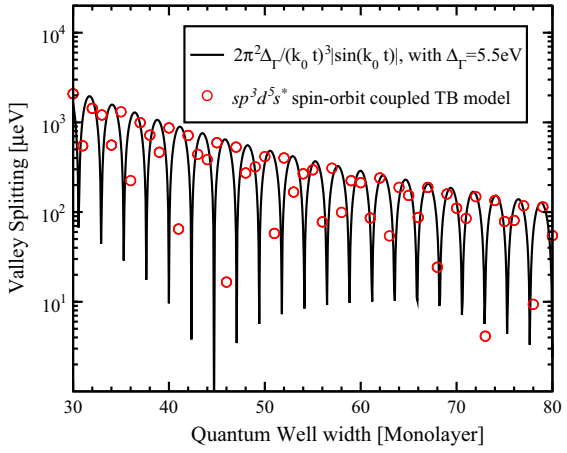

Fig. 6. Dependence of the valley splitting on the quantum well width from the tight binding (TB) model and the analytical expression with $\Lambda_\Gamma = 5.5$ eV.

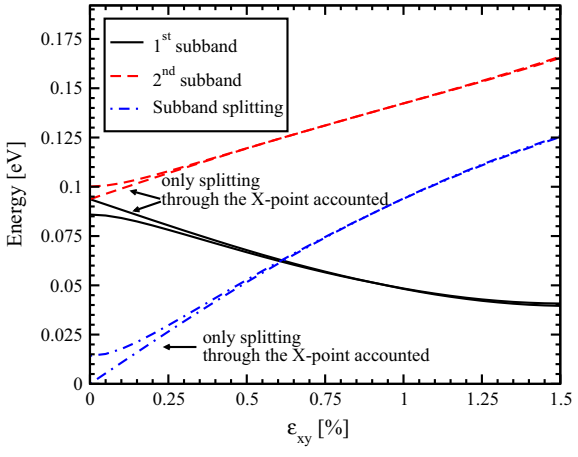

Fig. 7. Dependence of the energy of the 1st and the 2nd subbands together with the subband splitting on shear strain for the film thickness 2.1 nm.

The calculation of the conduction electron spin relaxation due to surface roughness and electron–phonon scattering in (001) silicon films starts from properly taking into account the valley degeneracy lifting in unstrained films. The [001] equivalent valley

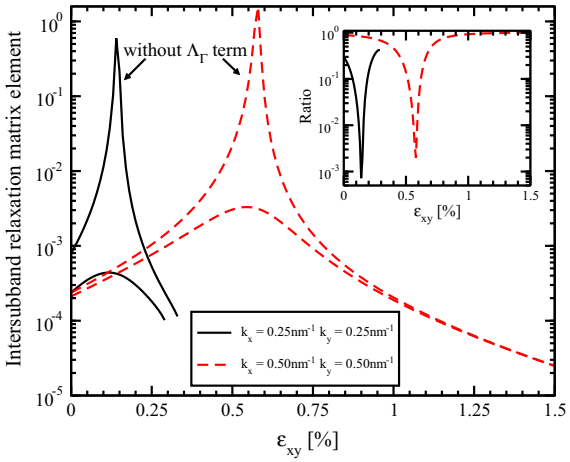

Fig. 8. Dependence of the normalized intersubband relaxation matrix elements on shear strain for the film thickness 2.1 nm. The inset shows the ratio of the matrix elements with the Λ_Γ term to the matrix elements without the Λ_Γ term.

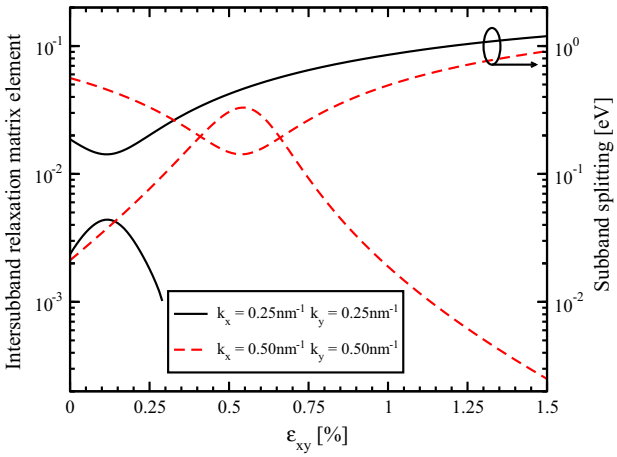

Fig. 9. Dependence of the normalized intersubband relaxation matrix elements on shear strain for the film thickness 2.1 nm. The inset shows the ratio of the matrix elements with the Λ_Γ term to the matrix elements without the Λ_Γ term.

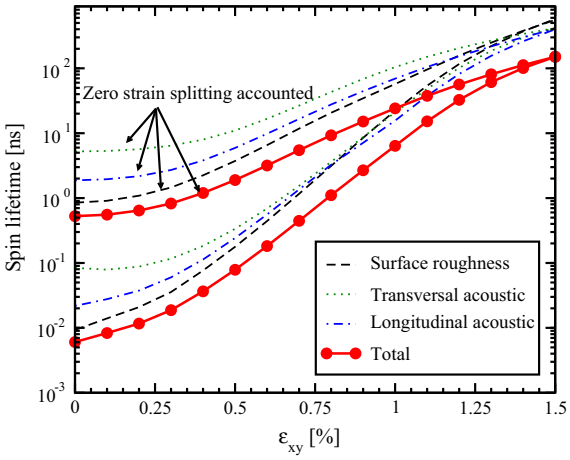

Fig. 10. Dependence of spin lifetime on shear strain for T = 300 K and film thickness 2.1 nm.

coupling through the Γ-point results in a subband splitting in confined electron structures [11]. The values of the valley splitting

obtained from a 30-band $\mathbf{k}\cdot\mathbf{p}$ model [12], an atomistic tight-binding model from [13], and from [14] are shown in Fig. 5. Although looking irregular, the results follow a certain law. Fig. 6 demonstrates a good agreement of the results of the tight-binding calculations with the analytical expression for the subband splitting [1]

$$\Lambda_\Gamma = \frac{2\pi\Delta_\Gamma}{(k_0 t)^3}\sin(k_{0\Gamma}t), \tag{17}$$

where Δ_Γ is the splitting at Γ-point, $k_{0\Gamma} = 0.85\frac{2\pi}{a}$, a is the lattice constant, and t is the film thickness. The good agreement is found for the value Δ_Γ = 5.5 eV.

Fig. 7 shows the dependence of the lowest unprimed subbands' energies and their splitting on shear strain with and without accounting for the Λ_Γ term. The unprimed subbands are degenerate at zero strain without the Λ_Γ term. The Λ_Γ term lifts the degeneracy while shear strain gives the major contribution to the splitting at high strain values. The surface roughness scattering matrix elements are taken to be proportional to the square of the product of the subband wave function derivatives at the interface [11]. The surface roughness intersubband spin relaxation matrix elements with and without the Δ_Γ term are shown in Fig. 8. The difference in the matrix elements' values calculated with and without the Δ_Γ term (inset Fig. 8) can reach two orders of magnitude. Hence, the valley coupling through the Γ-point must be taken into account for accurate spin lifetime calculations.

The peaks on the matrix elements' dependencies (Fig. 8) are correlated with the unprimed subband splitting minima (Fig. 9). For higher strain values these peaks, corresponding to strong spin relaxation hot spots, are pushed towards unoccupied states at higher energies (Fig. 9). This leads to the strong increase of the spin lifetime demonstrated in Fig. 10. The increase is less pronounced, if the Λ_Γ term responsible for the valley splitting in relaxed films is taken into account. However, even in this case the spin lifetime is boosted by almost two orders of magnitude.

4. Conclusion

We have presented an approach to evaluate mobility and spin lifetime in strained ultra-thin silicon films. We have shown that the usually neglected surface roughness matrix scattering elements' dependence on strain makes it possible to double the electron mobility in stressed thin silicon films. We have demonstrated a strong, almost two orders of magnitude, increase of spin lifetime in strained silicon films. Thus shear strain used to boost mobility can also be used to increase spin lifetime.

Acknowledgments

This work is supported by the European Research Council through the Grant #247056 MOSILSPIN. The computational results have been achieved in part by using the Vienna Scientific Cluster (VSC).

References

[1] Sverdlov V. Strain-induced effects in advanced MOSFETs. Springer; 2011.
[2] Sugahara S, Nitta J. Spin transistor electronics: an overview and outlook. Proc IEEE 2010;98(12):2124–54.
[3] Datta S, Das B. Electronic analog of the electro-optic modulator. Appl Phys Lett 1990;56:665.
[4] Jansen R. Silicon spintronics. Nat Mater 2012;11:400–8.
[5] Li J, Appelbaum I. Modeling spin transport in electrostatically-gated lateral-channel silicon devices: role of interfacial spin relaxation. Phys Rev B 2011;84:165318.
[6] Li P, Dery H. Spin-orbit symmetries of conduction electrons in silicon. Phys Rev Lett 2011;107:107203.
[7] Osintsev D, Baumgartner O, Stanojevic Z, Sverdlov V, Selberherr S. Subband spitting and surface roughness induced spin relaxation in (001) silicon SOI MOSFETs. Solid-State Electron. 2013;90:34.
[8] Song Y, Dery H. Analysis of phonon-induced spin relaxation processes in silicon. Phys Rev B 2012;86:085201.
[9] Fischetti MV, Ren Z, Solomon PM, Yang M, Rim K. Six-band $\mathbf{k}\cdot\mathbf{p}$ calculation of the hole mobility in silicon inversion layers: dependence on surface orientation, strain, and silicon thickness. J Appl Phys 2003;94:1079.
[10] Osintsev D, Sverdlov V, Selberherr S. Reduction of momentum and spin relaxation rate in strained thin silicon films. Proc of the 43rd ESS-DERC; 2013, p. 334–7.
[11] Ando T, Fowler AB, Stern F. Electronic properties of two-dimensional systems. Rev Mod Phys 1982;54:487.
[12] Rideau D, Feraille M, Michaillat M, Niquet YM, Tavernier C. On the validity of the effective mass approximation and the Luttinger $\mathbf{k}\cdot\mathbf{p}$ model in fully depleted SOI MOSFETs. Solid-State Electron 2009;53:452.
[13] Nestoklon MO, Golub LE, Ivchenko EL. Spin and valley-orbit splittings in SiGe/Si heterostructures. Phys Rev B 2006;73:235334.
[14] Osintsev D, Sverdlov V, Neophytou N, Selberherr S. Valley splitting and spin lifetime enhancement in strained silicon heterostructures. Proc of 18th intl winterschool on new developments in solid state physics 2014, p. 88–9.